Available online at www.sciencedirect.com
ScienceDirect
Journal of Power Sources 174 (2007) 689–694
JOURNAL OF POWER SOURCES
www.elsevier.com/locate/jpowsour

Short communication

Electrical conductivity and reaction with lithium of $LiFe_{1-y}Mn_yPO_4$ olivine-type cathode materials

J. Molenda *, W. Ojczyk, J. Marzec

Faculty of Materials Science and Ceramics, AGH University of Science and Technology, al. Mickiewicza 30, 30-059 Krakow, Poland

Available online 3 July 2007

Abstract

Structural, electrical and electrochemical properties of Mn-substituted phospho-olivines $LiFe_{1-y}Mn_yPO_4$ were investigated and compared to those of $LiFePO_4$. Rietveld refined XRD patterns taken in the course of delithiation process showed apparent difference between phase compositions of these cathode materials upon lithium extraction. Contrary to the $LiFePO_4$ and $LiMnPO_4$ compositions for which a two-phase mechanism of electrochemical lithium extraction/insertion is observed, in case of Mn-substituted $LiFe_{1-y}Mn_yPO_4$ samples a single-phase mechanism of deintercalation was observed in the studied range of lithium concentration. Electrochemical characterization of the cathode materials were performed in $Li/Li^+/Li_xFe_{1-y}Mn_yPO_4$-type cells for $y = 0.0$, 0.25, 0.55, 0.75 and 1.0 compositions. Voltammery studies showed low reversibility of the lithium extraction process in the high-voltage "manganese" range, while in the "iron" range the reversibility of lithium extraction is high. Impedance measurements of the $LiFe_{1-y}Mn_yPO_4$ cathode materials, which enabled separation of the ionic and electronic components of their entire electrical conductivity, showed distinct influence of Mn content on the electronic part of conductivity. EIS measurements performed at different states of cell charge revealed that the charge-transfer impedance in $Li_xFe_{1-y}Mn_yPO_4$ is much lower than that of Li_xFePO_4.

Keywords: Phospho-olivines; $LiFe_{1-y}Mn_yPO_4$; Intecalation; Two-phase electrode reaction; Cyclic voltammetry; EIS

1. Introduction

Phosphate-based materials have recently attracted considerable interest as a promising new class of cathode materials in *Li-ion* batteries for large-scale applications. Among them particularly the $LiFePO_4$ with olivine structure as well as isostructural compounds, such as $LiFe_{1-y}Mn_yPO_4$ ($0 \le y \le 1$) are in the center of attention. The main advantages of the $LiFePO_4$ are high-volumetric capacity (170 mAh g^{-1}), high and flat voltage profile (~3.4 V versus Li/Li^+), thermal stability and environmental benign. Nevertheless there is serious drawback arising from its almost insulating properties, as electrical conductivity of $LiFePO_4$ is of the order of 10^{-10} S cm^{-1} at RT. Since any effectively working cathode material requires high-electronic conductivity and fast diffusion of lithium ions, many efforts have been undertaken to improve properties of these based cathode materials. Most of them were concentrated on significant increase of macroscopic electrical conductivity, either by optimization of microstructure and usage of carbon additives to the cathode material [1–4] or, alternatively, by obtaining electronically conductive phospho-olivine [5]. Low concentration of electronic carriers in stoichiometric $LiFePO_4$ and structural restrictions (one dimensional paths for lithium diffusion) are responsible for limitation of the kinetics of lithium extraction process. A two-phase mechanism of lithium extraction/insertion, as is observed in working $Li/Li^+/Li_xFePO_4$ cell, is described by the following equation:

$$LiFePO_4 - (1-x)Li^+ - (1-x)e^- \leftrightarrow xLiFePO_4 + (1-x)FePO_4. \quad (1)$$

Yamada et al. [6–8] have reported, that by means of chemical method of lithium extraction of $Li_xFe_{1-y}Mn_yPO_4$ at voltage of ~3.5 V, the reaction proceeds as follows:

$$LiFe_{1-y}Mn_yPO_4 - (1-x)Li^+ - (1-x)e^- \leftrightarrow Li_xFe_{1-y}Mn_yPO_4, \quad (2)$$

where $y \le x \le 1$. Reaction at this voltage is related to the oxidation of iron $Fe^{2+} \rightarrow Fe^{3+}$. At 4.1 V, when manganese oxidation

* Corresponding author.
E-mail address: molenda@agh.edu.pl (J. Molenda).

0378-7753/$ – see front matter © 2007 Elsevier B.V. All rights reserved.
doi:10.1016/j.jpowsour.2007.06.238

takes place, $Mn^{2+} \rightarrow Mn^{3+}$, the mechanism of reaction changes and a two-phase product is obtained according to the following equation

$$Li_yFe_{1-y}Mn_yPO_4 - (y-x)Li^+ - (y-x)e^- \leftrightarrow xLi_xFe_{1-y}Mn_yPO_4 + (y-x)Fe_{1-y}Mn_yPO_4, \quad (3)$$

where $0 \le x \le y$. The process described by Eq. (2) is remarkably different from delithiation of $LiFePO_4$ or $LiMnPO_4$, for which, in almost the whole range of lithium content, a two-phase mechanism of electrochemical lithium extraction/insertion is observed (i.e. according to Eq. (1)).

The objective of this work was to determine structural, electrical and electrochemical properties of Mn-substituted phospho-olivines $LiFe_{1-y}Mn_yPO_4$ ($y = 0.0, 0.25, 0.55, 0.75, 1.0$) investigated in the course of electrochemical delithiation process with comparison to those of $LiFePO_4$.

2. Experimental

The $LiFe_{1-y}Mn_yPO_4$ ($y = 0.0, 0.25, 0.55, 0.75, 1.0$) samples were synthesized by a high-temperature solid-state reaction, using Li_2CO_3 (POCH, ppa), $FeC_2O_4{\cdot}2H_2O$ (Sigma–Aldrich, ppa), $NH_4H_2PO_4$ (POCH, ppa) and $MnCO_3$ (Sigma–Aldrich, ppa). The precursors were weighed according to the stoichiometric ratio, thoroughly ground for 2 h by ball milling with acetone added, then dried and pressed into pellets. The initial heating and synthesis were performed in a high purity (5N) argon flow with heating up to 350 °C at slow rate (to remove all gaseous products) followed by final heating performed at 750 °C for 24 h. The samples were characterized by X-ray powder diffraction analysis using Cu Kα radiation (Philips X'Pert Pro), X-ray spectra were analyzed by Rietveld method using the X'Pert Pro software. Electrochemical characterization of the cathode materials was carried out in electrochemical cells $Li/Li^+/Li_xFe_{1-y}Mn_yPO_4$. The electrolyte was a 1 M solution of $LiClO_4$ in 1:1 ethylene carbonate/dimethyl carbonate (EC/DEC). $LiFe_{1-y}Mn_yPO_4$ powders were mixed with carbon black and PVDF with weight proportion 7.5:2:0.5 and then dissolved in organic solvent NMP. The slurry was then cast onto Al foil and dried at 120 °C in vacuum dryer. The positive electrode was in the form of a circular 12 mm diameter 1 mm thin disc.

Voltammetry curves in the course of charge and discharge for the cells $Li/Li^+/Li_xFe_{1-y}Mn_yPO_4$ ($y = 0.0, 0.25, 0.55, 0.75, 1.0$) were recorded in the 2.5–4.6 V range. The cells were studied by impedance spectroscopy method at different states of charge with use of Autolab PGSTAT302 with FRA module. The applied frequency range was from 10^{-3} to 10^3 Hz, with the amplitude of overpotential equal to 0.01 V.

3. Results and discussion

Fig. 1 shows XRD patterns of the series of synthesized $LiFe_{1-y}Mn_yPO_4$ samples. The crystal structure of all the samples exhibits a single-phase olivine-type orthorhombic *Pnma* structure.

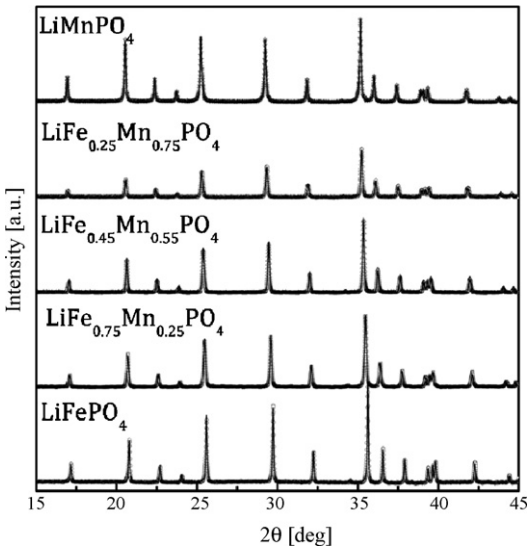

Fig. 1. XRD patterns of $LiFe_{1-y}Mn_yPO_4$ samples. The solid line connecting points is fitted with Rietveld method.

As expected, substitution of Fe^{2+} (0.92 Å) at the 4c site by Mn^{2+} (0.97 Å) cations causes an increase of the cell parameters, according to Vegard's law. Lattice parameters obtained from Rietveld refinement and corresponding values of the *S* coefficient are shown in Table 1.

The OCV curves of $Li/Li^+/Li_xFe_{1-y}Mn_yPO_4$ ($y = 0.0, 0.25, 0.55, 0.75, 1.0$) cells are presented in Fig. 2. For samples containing both iron and manganese two characteristic potential plateaux are observed. The first one, at the voltage of ~3.6 V versus Li/Li^+ is related to the iron oxidation $Fe^{2+} \rightarrow Fe^{3+}$, while the second one close to 4.1 V is related to the manganese oxidation $Mn^{2+} \rightarrow Mn^{3+}$. The steep change of voltage by about 0.5 V is observed at lithium content *x* equal to manganese concentration *y* in $LiFe_{1-y}Mn_yPO_4$ and reflects the difference of position of the Fermi level between the iron and the manganese redox couples in the cathodes. For comparison sake in Fig. 2 the analogous OCV curves, obtained for cells with $LiMnPO_4$ and $LiFePO_4$ cathode materials are presented. The value of the voltage at which the iron oxidation $Fe^{2+} \rightarrow Fe^{3+}$ takes place in $LiFePO_4$ compound is lower (~0.1 V) than this observed for materials containing manganese. Padli et al. [9] explained this phenomenon on a basis of a superexchange interaction between Fe–O–Mn ions.

The temperature dependences of the electronic and ionic conductivity of $LiFePO_4$, $LiFe_{0.25}Mn_{0.75}PO_4$ and $LiFe_{0.45}Mn_{0.55}PO_4$ are shown in Fig. 3a and b, respectively. The

Table 1
Lattice parameters and Rietveld coefficients of synthesized $LiFe_{1-y}Mn_yPO_4$ samples

y in $LiFe_{1-y}Mn_yPO_4$	*a* (Å)	*b* (Å)	*c* (Å)	$S = R_{wp}/R_p$
0.0	10.3284 (1)	6.007 (1)	4.6925 (2)	1.2678
0.25	10.3568 (2)	6.0297 (9)	4.7058 (8)	1.3246
0.55	10.3958 (1)	6.0576 (7)	4.7203 (6)	1.2865
0.75	10.421 (1)	6.0799 (5)	4.7331 (7)	1.2934
1.0	10.4481 (2)	6.1034 (1)	4.7454 (1)	1.5219

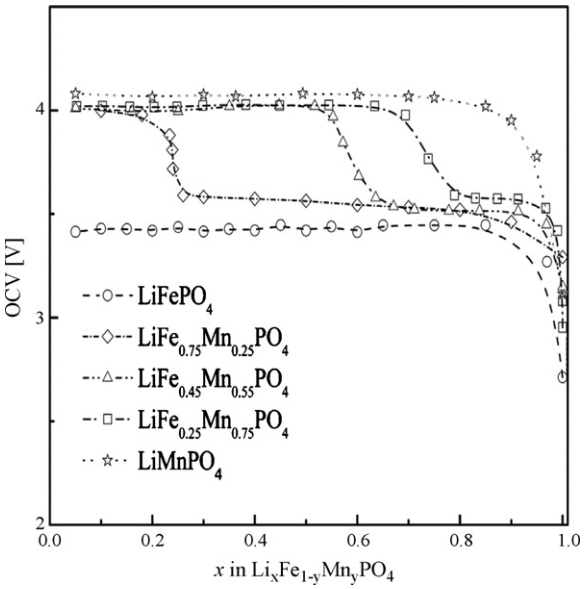

Fig. 2. OCV curves of $Li/Li^+/Li_xFe_{1-y}Mn_yPO_4$ cells.

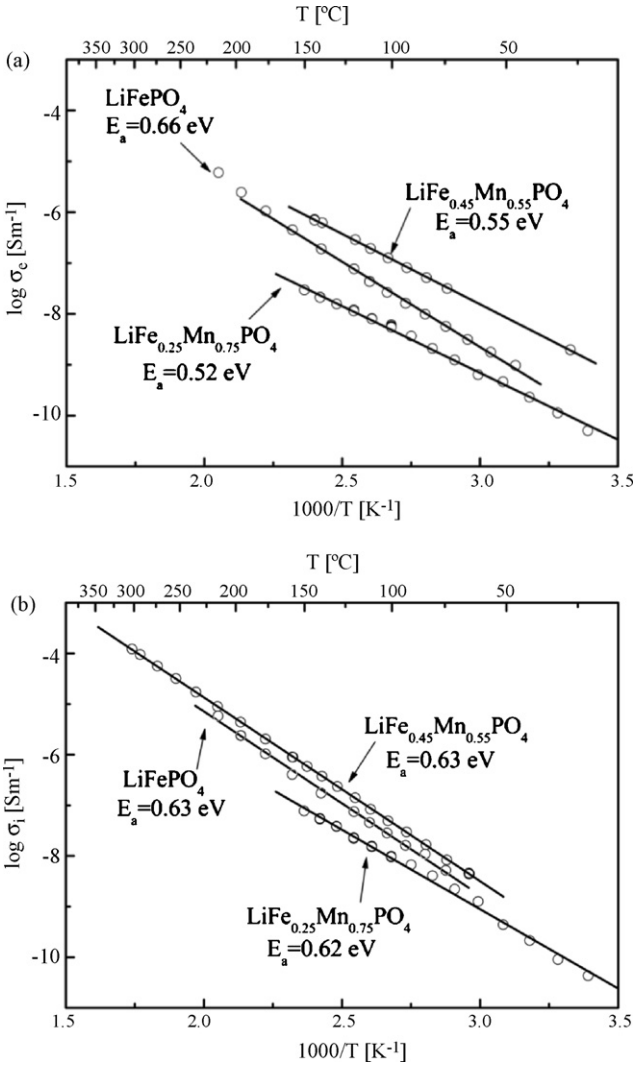

Fig. 3. Electronic (a) and ionic (b) components of electrical conductivity of selected $LiFe_{1-y}Mn_yPO_4$ samples.

electronic component of conductivity of the $LiFe_{0.45}Mn_{0.55}PO_4$ sample is distinctly higher as compared with the $LiFePO_4$ and also activation energies for the Mn containing samples are lower, which can be related to the presence of Fe^{2+}–Mn^{2+} pairs (Fig. 3a). The ionic components determined for $LiFePO_4$ and manganese including samples as well as their activation energies do not differ considerably (Fig. 3b). The rather slight influence of manganese on conductivity is due to charge transport via Fe–O–Mn bond, which was already discussed [10].

The evolution of crystallographic cell parameters of deintercalated $Li_xFe_{0.45}Mn_{0.55}PO_4$ samples, as a function of lithium content is presented in Fig. 4a and b shows XRD patterns

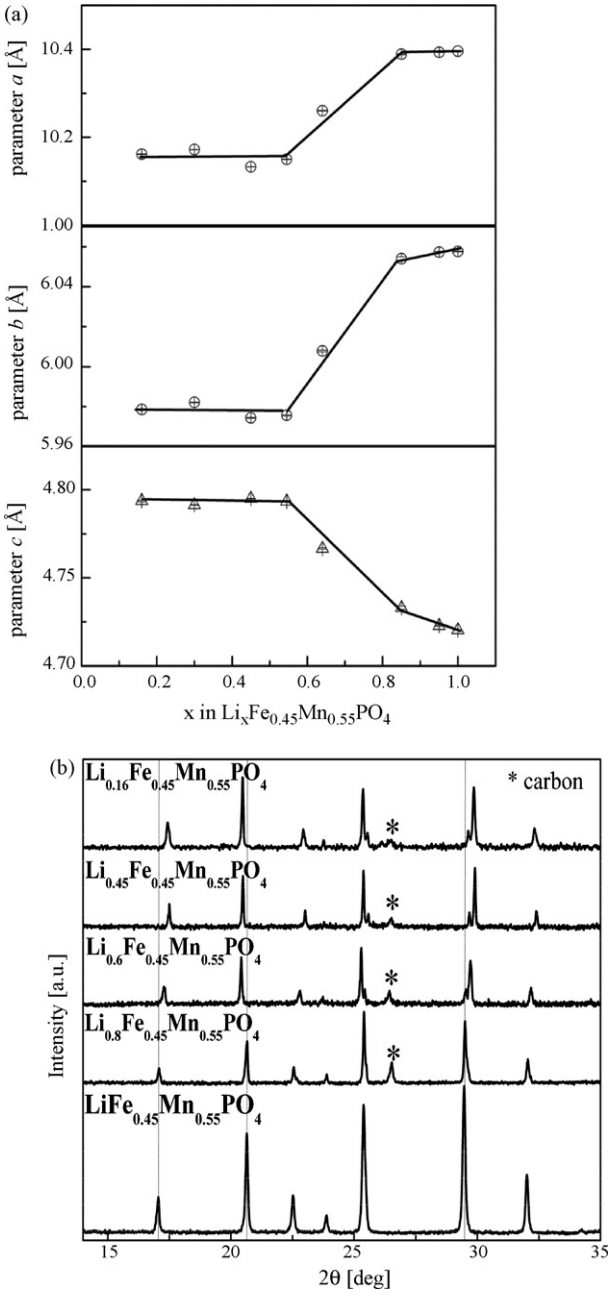

Fig. 4. (a) Evolution of crystallographic cell parameters of deintercalated $Li_xFe_{0.45}Mn_{0.55}PO_4$ samples and (b) corresponding XRD patterns of the cathode material at different stages of electrochemical deintercalation.

obtained for the cathode material at different stages of electrochemical deintercalation in a Li/Li$^+$/Li$_x$Fe$_{0.45}$Mn$_{0.55}$PO$_4$ cell. From the figure it is known that the material remains single phase in the whole Li content range ($x = 1.0$–0.16). For the lithium content, where the cell voltage is ~3.5 V and iron oxidation $Fe^{2+} \rightarrow Fe^{3+}$ takes place, a monotonous variation of the *a*, *b*, and *c* lattice parameters of the phospho-olivine with lithium content is observed up to lithium content $x = 0.55$. When lithium concentration decreases below 0.55, the XRD patterns still indicate a single-phase material, but surprisingly the lattice parameters remain constant. This can be explained by the model developed by Andersson and Thomas [11], according to which delithiation of the phospho-olivines does not proceed by a radial mode but by a mosaic mode, involving appearance of microregions with and without lithium in the cathode material.

Opposing to these results, Yamada et al. [9–11] have shown for Li$_x$Fe$_{1-y}$Mn$_y$PO$_4$ ($y = 0.2, 0.4, 0.6, 0.8$) samples, that delithiation is a single-phase process at 3.5 V, while at 4 V the manganese oxidation $Mn^{2+} \rightarrow Mn^{3+}$ leads to formation of two phases. This disagreement however should be related to the fact that in Yamada's experiments lithium was extracted in a different way—chemically in NO_2BF_4 solution. Therefore such a divergent behavior should be attributed to the different lithium extraction methods. This can be expected, as it was shown earlier [12] in the case of manganese spinel $LiMn_2O_4$ deintercalation by electrochemical and chemical methods yield materials of different physical and chemical properties. For comparison sake in Fig. 5 analogous XRD measurements are presented for the $LiFePO_4$ cathode material. In this case it is visible that the delithiation process goes on via two-phase mechanism and the variation of the lattice parameters are within experimental error.

Fig. 6 shows series of Nyquist plots of the Li/Li$^+$/Li$_x$Fe$_{1-y}$Mn$_y$PO$_4$ ($y = 0.0$, 0.25, 0.55, 0.75) cells taken in the course of battery charging process. It can be seen that the Nyquist plots are comprised of at least two depressed semicircles in high- and low-frequency range and a line inclined at almost constant angle to the real axis in the low-frequency range. The semicircles, which are to some extent overlapped, have a high-frequency cutoff that identifies the ohmic resistance of the electrolyte and electrodes. At lower frequencies, the resistance is related to the complex reaction process of charge transfer between the electrolyte and the active material, i.e. migration of the Li^+ ions at the electrode/electrolyte interface and interparticle contact resistance. The second, low frequency arc, which is less or more pronounced, is probably related to the varying thickness of surface layer on the lithium anode. In every spectrum at very low frequencies, there is a third region in which the impedance spectra showed a typical Warburg behavior (straight line) which is attributed to the diffusion of lithium ions in the bulk of the cathode material. The observed evolution of the impedance spectra during charging reflects the intrinsic changes a cell undergoes. The size of the higher frequency semicircle apparently changes with the charging process which can be explained by the development of lithium ions diffusing paths due to the permeation of electrolyte through cathode material during charging. This yields more active reaction sites and effectively the reaction resistance on the electrolyte/cathode

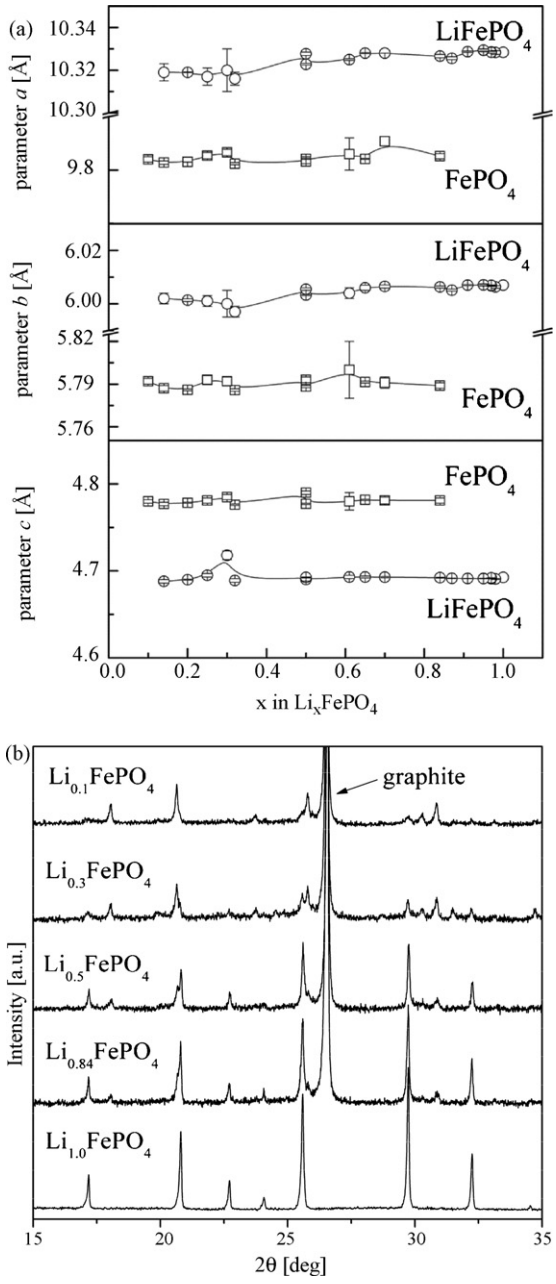

Fig. 5. (a) Cell parameters of deintercalated Li$_x$FePO$_4$ samples and (b) corresponding XRD patterns of the cathode material at different stages of electrochemical deintercalation.

interface decreases. Generally the charge-transfer impedance of Li$_x$Fe$_{1-y}$Mn$_y$PO$_4$ is much lower than that of $LiFePO_4$. In case of the Li/Li$^+$/Li$_x$Fe$_{1-y}$Mn$_y$PO$_4$ cells it is worth noting the change of the Warburg component in the vicinity of the potential jump on the OCV curve. It virtually disappears reflecting the change in the cell operation and electronic conductivity mechanism (Mn^{2+}/Mn^{3+} instead of Fe^{2+}/Fe^{3+}).

First charge/discharge voltammogram curves together with corresponding charge/discharge curves are presented in Fig. 7. For the $LiFePO_4$ and $LiMnPO_4$ samples, only a pair of anodic and cathodic peaks is observed. The average peak value for $LiFePO_4$ is 3.45 V and 4.1 V for $LiMnPO_4$. The difference

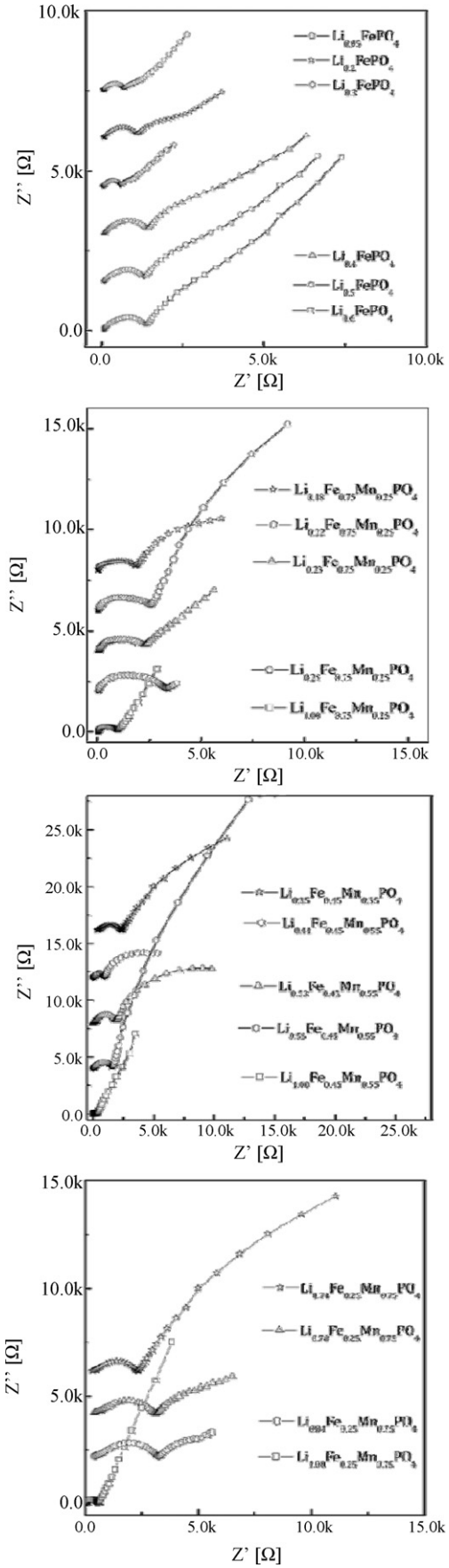

Fig. 6. EIS spectra of the Li/Li$^+$/Li$_x$Fe$_{1-y}$Mn$_y$PO$_4$ (y = 0.0, 0.25, 0.55, 0.75) cells taken at different stages of charge x.

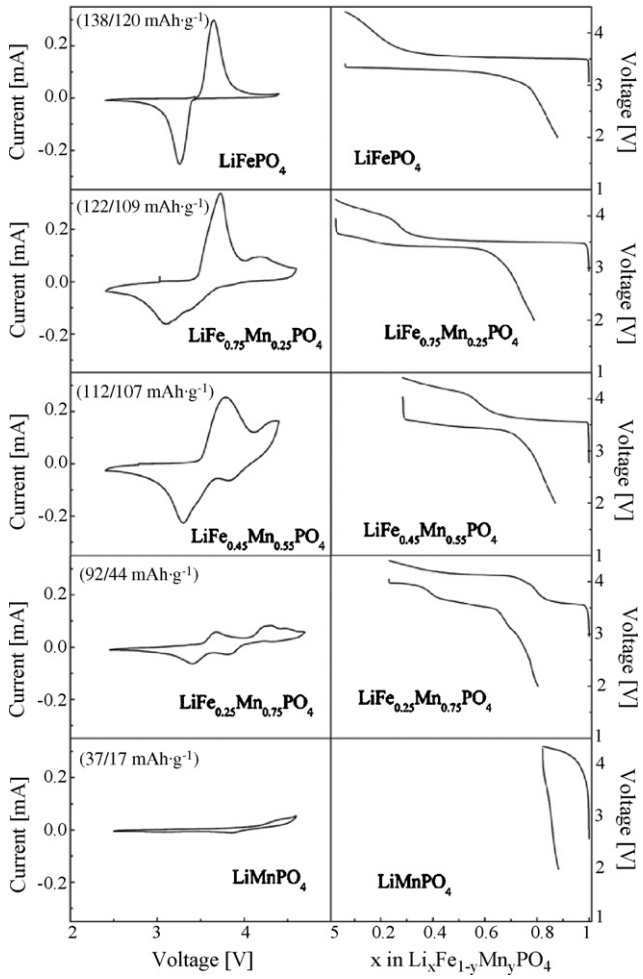

Fig. 7. First voltammetric cycles of the Li/Li$^+$/Li$_x$Fe$_{1-y}$Mn$_y$PO$_4$ cells (2.5–4.6 V voltage range at 25 μV s^{-1} scan rate) together with corresponding charge/discharge curves under constant load of C/25. Values of obtained charge/discharge capacities are given in parentheses.

between the anodic and cathodic peaks' potential ΔE_p is 0.39 V for LiFePO$_4$ and 0.5 V for LiMnPO$_4$. It is rather high and indicates that there is a kinetic limitation in the electrochemical process. Concerning LiMnPO$_4$, the literature data are inconsistent: Padhi et al. [9] showed that they were unable to extract lithium from LiMnPO$_4$, Dominko et al. obtained ~25% reversibility [13] but Li et al. [14] achieved almost 90% of the theoretical reversible capacity of the material.

For manganese-substituted samples a decrease of the relative intensity of the iron peaks is observed while the intensity of the manganese peaks remains quite low for all compositions. The observed voltage of the iron oxidation/reduction process increases slightly for samples with higher manganese content and for the LiFe$_{0.25}$Mn$_{0.75}$PO$_4$ sample equals 3.55 V, which is in agreement with observed OCV voltages. The voltage of the manganese oxidation/reduction process is equal to 4.1 V and remains constant for all the compositions. For cells with LiFePO$_4$ and LiFe$_{0.75}$Mn$_{0.25}$PO$_4$ cathode materials almost full theoretical capacity during charge was observed. For LiFe$_{0.45}$Mn$_{0.55}$PO$_4$ and LiFe$_{0.25}$Mn$_{0.75}$PO$_4$ cathode materials about 70% of the theoretical capacity was achieved during first charge. It is worth

noting that during discharge the "manganese range" appears only for cathodes with high-manganese content while for other samples only the "iron reduction range" appears. Hence, the observed irreversible capacity (of about 10–20%) is mostly related to the "manganese range", while the "iron range seems" to be fully reversible. For $LiMnPO_4$ only about 20% of the theoretical capacity was achieved.

4. Conclusions

Substitution of iron with manganese in $LiFePO_4$ substantially changes the electrochemical performance of the olivine-type cathode material providing material in which properties are not simple assemblage of edging $LiFePO_4$ and $LiMnPO_4$ compositions. First a single-phase diffusional mechanism of deintercalation for Mn-substituted $LiFe_{1-y}Mn_yPO_4$ samples is observed in the whole range of lithium concentration, contrary to the pure $LiFePO_4$ and pure $LiMnPO_4$, where a two-phase mechanism of electrochemical lithium extraction/insertion is observed. Impedance measurements of the $LiFe_{1-y}Mn_yPO_4$ cathode materials, which enabled separation of the ionic and electronic components of their entire electrical conductivity, showed distinct influence of Mn content on the electronic part of conductivity. Nevertheless the first cycle reversibility of the lithium extraction process in the high-voltage oxidation (the "manganese range") is low, while in the "iron range" the reversibility of lithium extraction is high. The EIS measurements carried out for different state of cell charge indicated that the charge-transfer process in $Li_xFe_{1-y}Mn_yPO_4$ is much easier than that of Li_xFePO_4.

Acknowledgements

The work is supported by Polish Committee Scientific for Research under grant 4 T08A 020 25. The authors would like to thank Dr. M. Pałys for providing the Autolab PGSTAT302 with FRA module.

References

[1] H. Huang, S.-C. Yin, L.F. Nazar, Electrochem. Solid State Lett. 4 (2001) A170.
[2] Z. Chen, J.R. Dahn, J. Electrochem. Soc. 149 (2002) A1184.
[3] A. Yamada, M. Hosoya, S.-Ch. Chung, Y. Kudo, K. Hinokuma, K.-Y. Liu, Y. Nishi, J. Power Sources 119–121 (2003) 232.
[4] S. Franger, F. Le Cars, C. Bourbon, H. Rouault, J. Power Sources 119–121 (2003) 252.
[5] S.-Y. Chung, J.T. Bloking, Y.-M. Chiang, Nat. Mater. 1 (2002) 123.
[6] A. Yamada, Y. Kudo, S.-Ch. Chung, J. Electrochem. Soc. 148 (2001) 459, A960.
[7] A. Yamada, Y. Kudo, K.-Y. Liu, J. Electrochem. Soc. 148 (2001) A747.
[8] A. Yamada, Y. Kudo, K.-Y. Liu, J. Electrochem. Soc. 148 (2001) A1153.
[9] A.K. Padli, K.S. Nanjundaswamy, J.B. Goodenough, J. Electrochem. Soc. 144 (1997) 11884.
[10] J. Molenda, W. Ojczyk, K. Świerczek, W. Zając, F. Krok, J. Dygas, R.S. Liu, Solid State Ionics 177 (2006) 2617.
[11] A.S. Andersson, J.O. Thomas, J. Power Sources 97–98 (2001) 498.
[12] J. Molenda, W. Ojczyk, M. Marzec, J. Marzec, J. Przewoznik, Solid State Ionics 157 (1–4) (2003) 73.
[13] R. Dominko, M. Bele, M. Geberscek, M. Remskar, D. Hanzel, J.M. Goupli, S. Pejovnik, J. Jamnik, J. Power Sources 153 (2006) 274.
[14] G. Li, H. Azuma, M. Tohda, Electrochem. Solid State Lett. 5 (2002) A135.